




Modification of cellulose nanocrystals by self-assembly nucleation agents to improve poly(L-lactide) nanocomposite' properties

Shengxue Qin · Yanan Hu · Xiujuan Tian · Yang Tian · Weizhi Liu · Lifen Zhao 

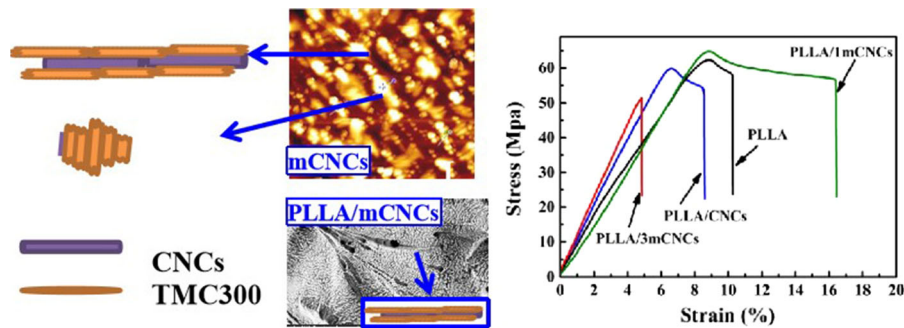
Received: 22 September 2019 / Accepted: 18 February 2020 / Published online: 29 February 2020
© Springer Nature B.V. 2020

Abstract The poor thermal stability of cellulose nano-crystals (CNCs) and dispersion in polymer matrices are significant obstacles limiting their applications in modification of polymers, especially during melt processing. The self-assembly nucleation agent, decamethylene dicarboxylic dibenzoyl hydrazide (TMC300), was used to modify CNCs via physical adsorption methods. Because TMC300 adsorbed on the surface of CNCs shields the sulfonate on CNCs, the thermal stability of CNCs was significantly improved. Meanwhile, modified CNCs formed different self-assembly morphologies in confined and unconfined spaces, which influenced the

crystallization behaviors and microstructures of poly(L-lactide) (PLLA). It improved the crystallization rate of PLLA, which increased the crystallinities and heat resistances of PLLA/CNC composites. More importantly, the self-assembly nucleation agent induced the shish-kebab structures of PLLA, which enhanced the interfacial structure as mechanically interfacial lock and simultaneously improved tensile strength and toughness. This physical and economical modification method of CNCs is anticipated to take full advantage of CNCs to modify PLLA or other semi-crystalline polymers via melt processing.

S. Qin · Y. Hu · X. Tian · Y. Tian · W. Liu · L. Zhao (✉)
School of Materials Science and Engineering, School of Mechanical and Electric Engineering, Shandong University of Science and Technology, Qingdao 266590, China
e-mail: lfzhao2009@126.com

Graphic abstract



Keywords Poly(L-lactide) · Cellulose nano-crystals (CNCs) · Self-assembly nucleation agent · Mechanical properties

Introduction

Increasing amounts of “white pollution” have made the research of biodegradable polymers an urgent requirement. Biodegradable poly(L-lactide) (PLLA) with good biocompatibility, thermal processing properties, relatively high strength, and renewable raw materials, has been deemed one of the most important biodegradable polymers, which can be potentially used in medical or industrial products (Dash and Konkimalla 2012; Ramot et al. 2016; Snell and Peoples 2009; Lu et al. 2009). However, low crystallization rate, poor heat resistance, and excessive brittleness limit its wide range of potential applications (Li and Huneault 2007; Al-Itry et al. 2012; Bhardwaj and Mohanty 2007). Cellulose nano-crystals (CNCs) are ideal to modify PLLA (Morin and Dufresne 2002; Petersson et al. 2007; Samir et al. 2004; Helbert et al. 1996), as they are natural renewable nanoparticles with biodegradability, high elastic modulus (approximately 143 GPa) (Šturcova et al. 2005), and good gas barrier property (Dhar et al. 2015; Fortunati et al. 2012; Fang et al. 2019). Unfortunately, CNCs are usually prepared via sulfuric acid hydrolysis and certain sulfate groups remain on their surfaces, which generate sulfuric acid upon heating and thus significantly diminish the thermal stability of the crystals during melt processing (Liu et al. 2017; Roman and Winter 2004; Wang et al. 2007). Besides this problem, the poor dispersion of

CNCs, caused by their inner hydrogen bonding, and their poor compatibility with polymer matrices greatly limit their efficiency in modifying PLLA.

To achieve the full potential of CNCs in modifying polymer, significant efforts have been devoted to improving its thermal stability by removing the sulfate groups via mild acid hydrolysis (Cheng et al. 2017), alkaline treatment (Nan et al. 2017), solvolysis (Tan et al. 2015), or by shielding the sulfate groups by polymers via covalent grafting (Xie et al. 2018; Fang et al. 2019; Gan et al. 2019) or physisorption (Liu et al. 2017; Zhang et al. 2015). Among the aforementioned methods, the shielding strategy introduces organic groups on CNCs, which simultaneously promote its dispersion in matrices and enhance the interface between CNCs and polymers. To prepare this kind of CNCs, physisorption is an economical and effective method compared to the covalent grafting method (Raquez et al. 2012; Shojaeiarani et al. 2018) which is expensive and difficult to scale up. Several materials including surfactants (Mariano et al. 2017; Habibi 2014; Góis et al. 2019; Brinatti et al. 2016), long polyoxyethylene (PEO) chains (Azouz et al. 2013), block copolymers (Mano et al. 2017), graphene oxide (Montes et al. 2018; Pal et al. 2017), an imidazolium group (Mariano et al. 2017) or lignin etc. (Gupta et al. 2016, 2017) have been physically adsorbed on the surface of CNCs by virtue of hydrogen bonding or van der Waal interactions, achieving good dispersion and high thermal stability of CNCs in polymers.

Unfortunately, Boujemaoui compared physisorption and covalent grafting of poly(*n*-butyl methacrylate) (PBMA) on CNCs in PLLA/CNC composites and found that covalent grafting was superior to physisorption on modifying the thermal and mechanical properties of the composites (Boujemaoui et al. 2017). This

suggests that the interfacial interaction between physical modified CNCs and PLLA is still weaker than that of chemical modifications. Therefore, there is an urgent need to enhance the interface of physical modified CNCs and PLLA. Recently, a strategy of designing “mechanically interlocking” between polymer and fillers was proposed (Jin et al. 2014; Nie et al. 2014). For example, Nie et al. prepared root-like glass fibers (GF) and natural fibers (NF) by virtue of aryl amide-based nucleation agents in situ self-assembly in polypropylene (PP) melts (He et al. 2016; Huang et al. 2017). By this way, the self-assembly “roots” on fibers played a role of “mechanically interfacial lock” which effectively enhanced the interface of PP and GF or NF.

Many works have found that the self-assembly aryl amide-based nucleation agent exhibits significant nucleating ability for PLLA (Kong et al., 2019; Wen et al., 2010; Bai et al. 2011), and its amidogens are anticipated to form hydrogen bonds with the hydroxyl on the surface of CNCs according to existing literature (Incarnato et al., 1999; Choi et al. 2010). However, to the best of our knowledge, there is still no studies about modifying CNCs by the self-assembly nucleation agent to prepare its composites with PLLA. The self-assembly nucleation agent might impart some self-assembly structures on the CNCs which will play the role of “mechanically interfacial lock” and enhance the interface of PLLA and CNCs. Furthermore, the involvement of nucleation agent is expected to improve the crystallization rate of PLLA and consequently, improve the heat resistance which limits its applications.

Therefore, in the present work, the self-assembly nucleation agent of decamethylene dicarboxylic dibenzoyl hydrazide (TMC300) are used to prepare modified CNCs (mCNCs) via physisorption to improve the thermal stability of CNCs, and take advantage of the distinct self-assembly properties of TMC300 to enhance the interface of PLLA/CNC composites. PLLA/mCNCs composites were prepared via melt blending, and their crystallization behaviors, mechanical properties, and heat resistances were investigated. Compared with the PLLA/CNCs, PLLA/mCNCs composites exhibited different crystallization morphologies, high crystallization rates, improved mechanical properties, and heat resistance. This work proposes a physical method to carry out the melt processing of CNCs, improve the crystallization

behaviors of PLLA and enhance the interfacial structure of PLLA/CNC composites, simultaneously.

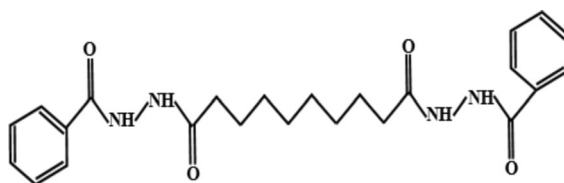
Experimental

Materials

Commercially available PLLA (4032D, Nature Works) with high stereoregularity (1.2–1.6% D-isomer lactide) was used in this study. The weight-averaged molecular weight and polydispersity were 207 kDa and 1.74, respectively. Cotton linter pulps (CLP) were purchased from a local market. Sulfuric acid (H_2SO_4 , 98 wt%, analytically pure), sodium hydroxide (NaOH, analytically pure) were purchased from Shanghai Pilot Chemical Corporation. Dimethyl sulfoxide (DMSO, analytically pure) was bought from Chengdu Kelon Chemical Reagent Factory. Decamethylene dicarboxylic dibenzoyl hydrazide (TMC300, chemical structure is depicted in Scheme 1) with a melting temperature of approximately 375 °C was supplied by Shanxi Provincial Institute of Chemical Industry, China.

Preparation and surface modification of CNCs

CNCs were prepared via sulfuric acid hydrolysis according to the method discussed in the following reference (Abitbol and Kloser 2013). During the typical procedure, CLPs were soaked overnight in sodium hydroxide of 4% in weight ratio at 25 °C. The obtained slurry was washed with deionized water until a pH of 7 was achieved, and then dried at 60 °C in a vacuum oven for 24 h. Subsequently, the pretreated slurry was hydrolyzed in 64 wt% sulfuric acid at 44 °C for 180 min with continuous stirring. Then, the reaction was stopped by applying ten-fold volumes of deionized water, and the resulting suspension was centrifuged and repeatedly washed until it could not be



Scheme 1 Chemical structure of TMC300

stratified. After dialyzing against deionized water until a pH value of 7 was achieved, the CNCs were obtained by freeze-drying and sieving.

Modified CNCs were prepared via physisorption. The CNCs and the nucleating agent TMC300 were dissolved in a certain amount of dimethyl sulfoxide (DMSO) via ultrasonication for 60 min. Then, the mixture was vacuum filtered using a 0.15 μm micro-porous film to remove the un-adsorbed TMC300. The filter cake was dried in a vacuum oven at 60 °C for 12 h. After sieving, the mCNCs with CNCs/TMC300 raw weight ratios of 1/1 or 1/2 were prepared and their production yields were approximately 60% and 45%, respectively. The actual contents of TMC300 in mCNCs were calculated by the following equation:

$$\text{Content}_{(\text{TMC300})} = \frac{W_{\text{TMC300}} - (W_{\text{TMC300}} + W_{\text{CNCs}}) \times (1 - Y)}{(W_{\text{TMC300}} + W_{\text{CNCs}}) \times Y} \quad (1)$$

where W_{TMC300} and W_{CNCs} represent the raw weights of TMC300 and CNCs, respectively. “Y” is the production yields. Therefore, the actual contents of TMC300 are approximately 17 wt% and 25 wt% in mCNC samples with raw weight ratios of 1/1 or 1/2, respectively.

Preparation of PLLA/CNC and PLLA/mCNC nanocomposites

After being dried at 60 °C under vacuum for 24 h, PLLA, CNCs, and mCNCs were melt blended using an XSS-300 torque rheometer (Shanghai Kechuang Co. Ltd.) with a rotor speed of 50 rpm and 180 °C for 5 min. The PLLA/mCNCs composites, with the mCNC content of 1 wt% and 3 wt%, were prepared and coded as PLLA/1mCNCs and PLLA/3mCNCs. For comparison, PLLA, with 1 wt% pristine CNCs (denoted as PLLA/CNCs), were also prepared via the same melting process. During the investigation of crystallization behaviors, PLLA with 1 wt % TMC300 (PLLA/TMC300) samples were prepared via solution blending with chloroform (CHCl_3) as a solvent.

Characterizations

Atomic forced microscopy

CNCs and mCNCs were respectively dispersed in water and DMSO by ultrasonic dispersing. After spin

coating on the mica plate ($5 \times 5 \text{ mm}^2$), they were dried on a hot plate at 60 °C. The morphologies of CNCs and mCNCs were investigated by an atomic force microscope (AFM, Multimode 8, Bruker) in the tapping mode. Si tips (TESP) with a resonance frequency of approximately 300 kHz and a spring constant of about 40 Nm^{-1} were used. To obtain the sizes of the fabricated CNCs, a straight line was drawn along the length of the CNCs and the height profiles were obtained. The diameter and length were obtained according to the data in the vertical and horizontal axis, respectively.

Infrared spectroscopy analysis

Fourier transform infrared spectroscopy (FTIR) was used to analyze the structures of CNCs, TMC300 and mCNCs. The spectra were obtained at a constant spectral resolution of 4 cm^{-1} using a FTIR spectrometer (Nicolet 380, USA) in the wave number range of $4000\text{--}400 \text{ cm}^{-1}$ at 25 °C.

X-ray photoelectron spectroscopy

X-ray photoelectron spectroscopy (XPS) of CNC and mCNCs were measured on an X-ray photoelectron spectrometer (ESCALAB 250Xi). The C1s, O1s and N1s spectra were collected at pass energy of 20 eV with a scan step of 0.1 eV.

Thermo gravimetric analysis

Thermo gravimetric analysis (TGA) measurements were operated on a Mettler-Toledo simultaneous thermogravimetric analyzer (TGA/DSC1/1600LF). All analyses were carried out from 100 °C to 600 °C at a heating rate of 10 °C/min and under a nitrogen atmosphere with a flow rate of 50 mL/min.

Wide angle X-ray diffraction

The crystal structures of PLLA, PLLA/CNCs and PLLA/mCNCs were investigated by a wide angle X-ray diffractometer (WAXD) (RigakuD/Max2500PC) with nickel filtered Cu $K\alpha$ radiation (wave length = 0.154 nm, 40 kV, and 110 mA) in the 2θ range from 4° to 40° with scanning steps of 0.02°.

Differential scanning calorimetry

A Mettler-Toledo differential scanning calorimeter (TGA/DSC1/1600LF, Switzerland) was used to characterize the glass transition temperatures (T_g), crystallization temperatures (T_c) and melting temperature (T_m) of the nanocomposites. The samples were first heated to 200 °C at a heating rate of 10 °C/min and held for 3 min to erase the thermal history. After that, the samples were then quenched to 25 °C followed by the second heating to 200 °C at the same rate of 10 °C/min.

Scanning electron microscopy

The microstructures were observed by a scanning electron microscopy (SEM, Nova Nano SEM 450, FEI Co., Ltd.). The PLLA/CNC composites with varied compositions were cryogenically broken in liquid nitrogen and coated with gold in vacuum before observation.

Mechanical properties

Two kinds of samples—with and without crystallization—were prepared to investigate the mechanical properties. The thoroughly dried samples were placed in a mold of size $80 \times 80 \times 0.6 \text{ mm}^3$ and melted at 190 °C for 5 min at a pressure of 5 MPa. Samples of the first type were transferred quickly into ice water to obtain the samples without crystallization. Samples of the second type were naturally cooled to the room temperature of 25 °C to obtain samples with crystal structure. Following that, both kinds of samples were cut into dumbbell shapes to investigate their mechanical properties.

An electronic universal tensile strength testing equipment (AI-7000 M) was used to investigate the tensile properties of both kinds of aforementioned samples at 25 °C with a crosshead speed of 5 mm/min. The tensile data were recorded by averaging results over six replications.

The notched Izod impact strength test was performed on an XJJ-5 charpy impact tester (JinJian-test, China). The size of the rectangular specimen was $80 \times 10 \times 4 \text{ mm}^3$, and it included a U-shaped notch (of depth 1 mm). The average values of five specimens were used for data analysis.

Dynamic mechanical analysis

Dynamic mechanical analysis (DMA, DMA1) was then used to investigate the heat resistance of the crystal samples which were cut to $5 \times 25 \times 0.6 \text{ mm}^3$. The tensile mode (frequency = 1 Hz) was operated at temperatures range from 30 °C to 100 °C with a ϕ of 2 °C/min. The values of E' were obtained by averaging of the values of at least three replications.

Results and discussion

Characterization of CNCs and CNCs-TMC300

To intuitively exhibit the morphology changes effected by physisorption of TMC300, TEM and AFM images of CNCs and mCNCs have been depicted in Fig. 1. The TEM image in Fig. 1a₁ demonstrates the fact that pristine CNCs are rod-shaped and the modified CNCs, depicted in Fig. 1b₁, retain the rod-like morphologies. However, the diameters of mCNCs are evidently larger than that of the CNCs. According to the AFM images, depicted in Fig. 1a₂, a₃, the pristine CNCs have lengths of 200–300 nm and diameters of approximately 5 nm. After physisorption of TMC300, few pristine CNCs can be observed in Fig. 1b₂, and the diameters of most mCNCs increase to 5–10 nm (Fig. 1b₃, which suggests that the surfaces of CNCs are physically combined with TMC300. In addition, some black lines (labeled as blue arrows) are apparent in the image of mCNCs. Compared to the morphology of CNCs, most of these black lines with approximate lengths of 100–200 nm often appear as several short lines perpendicular to CNCs (as marked by “a” and “b”), and the rest with approximate lengths of 1.5 μm parallel to CNCs (as marked by “c”). Considering the self-assembly character of TMC300, these black lines can be attributed to the self-assembly structures of TMC300 combined on CNCs. These unique morphologies might bring changes about the structures and properties of CNCs.

Figure 2 depicts the FTIR spectra of CLP, CNCs, TMC300, and mCNCs with the compositions of CNCs/TMC300 being 1/1 and 1/2. For CLP and pristine CNCs, both exhibit characteristic peaks, including the intense O–H stretching vibration peak at 3343 cm^{-1} , the C–H stretching vibration peak at 2890 cm^{-1} , and the O–H bending vibration peak of

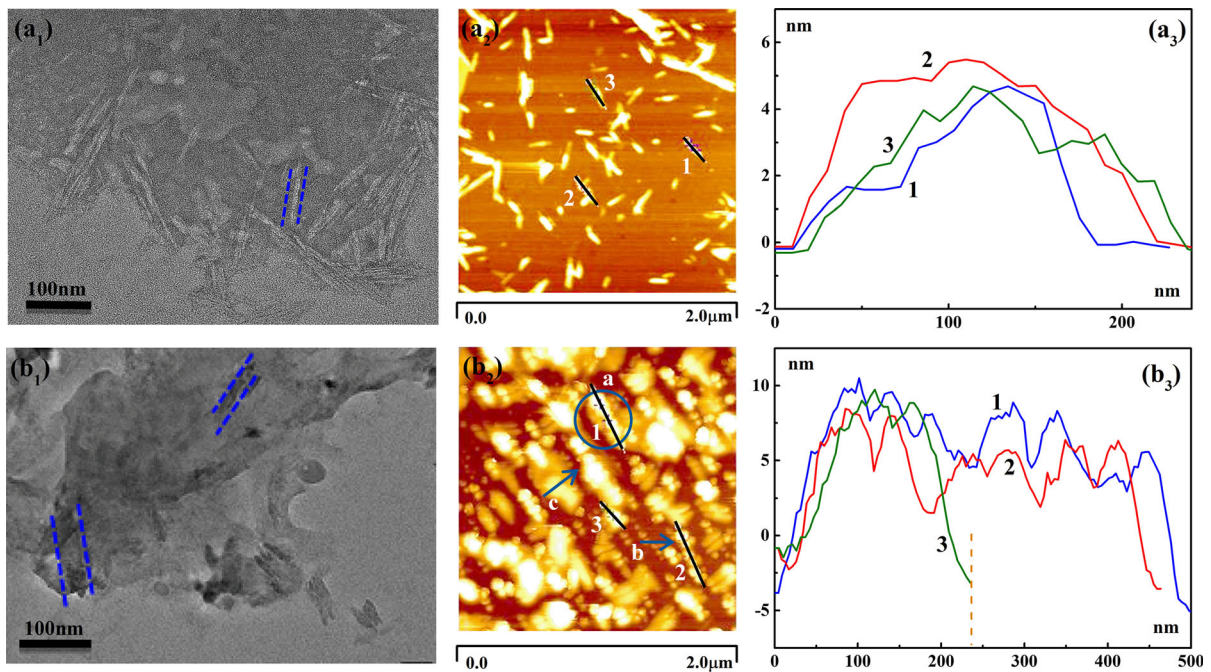


Fig. 1 TEM images of CNCs (**a₁**) and mCNCs (**b₁**). AFM height images of CNCs (**a₂**) and mCNCs (**b₂**). AFM height profiles of CNCs (image **a₃**) and mCNCs (image **b₃**)

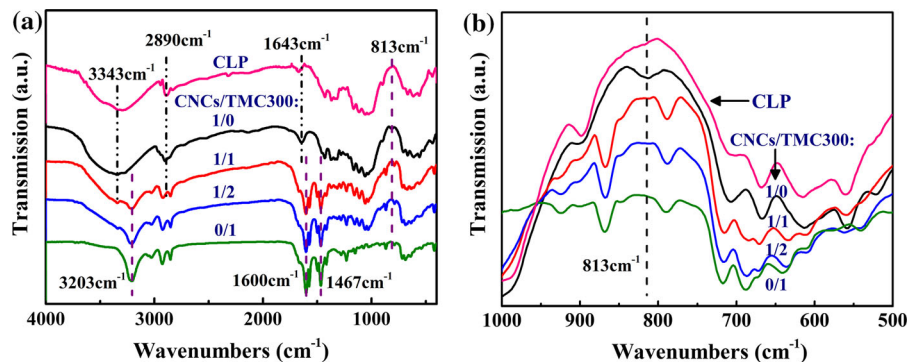


Fig. 2 FTIR of CLP, CNCs, TMC300 and mCNCs with the compositions of CNCs/TMC300: 1/1 and 1/2. **a** The wavenumbers range of 4000 cm⁻¹ to 400 cm⁻¹ and **b** enlargement in the wavenumbers range of 1000 cm⁻¹ to 500 cm⁻¹

adsorbed water at 1643 cm⁻¹ (Han et al. 2013; Yang et al. 2018). However, an additional peak is observed at 813 cm⁻¹, corresponding to symmetrical C-O-S vibration in CNCs (Börjesson et al. 2017), which suggests that the sulfonate was introduced during the preparation of the CNCs.

After physical modification by TMC300, the peaks of mCNCs at 3343 cm⁻¹ and 1643 cm⁻¹ became very weak. On the contrary, all characteristic peaks of TMC300 appear in the spectra of mCNC samples, including the N-H group at 3203 cm⁻¹, the C=O

stretching vibration at 1600 cm⁻¹, and the benzene skeletons vibration at 1467 cm⁻¹. However, the intensity of N-H group in mCNCs is evidently weaker than that of TMC300. Besides that, the methylene peaks are situated at 2920 cm⁻¹ and 2861 cm⁻¹, which are transformed into the same formations as those of TMC300. More importantly, the symmetrical C-O-S vibration at 813 cm⁻¹ disappears in the spectra of mCNCs, which indicates that sulfonates are no longer exposed to the surface due to the physisorption of TMC300. The shielding of sulfonate

is anticipated to improve the thermal stability of CNCs by avoiding the decomposition of sulfonate group at high temperature, which is the determinants of the thermal stability of CNCs (Voronova et al. 2013).

XPS measurement was carried out to further investigate the structures of CNCs and mCNCs. The elemental composition of the pristine CNCs and mCNCs have been listed in Fig. 3 and Table 1. As is apparent from Fig. 3a, peaks at approximately 536 eV and 290 eV can be distinctly observed in all samples, which correspond to O1s and C1s, respectively, revealing that oxygen and carbon are the major elements in the samples. For mCNC samples, the proportion of element O in the contents decreases from 67.2 to 35.8% and a distinct peak appears at approximately 404 eV corresponding to the element N in TMC300. Moreover, according to the high-resolution XPS spectra for pristine CNCs (Fig. 3b), three peaks can be observed at 282.4 eV (C–O–C), 284.5 eV (C–C and C–H), and 287.0 eV (C–O) (Xie et al. 2018; Bashar et al. 2019; Shi et al. 2019; Bao and Chrisey 2010), respectively. After modification by TMC300 (Fig. 3c), a peak appears at 288.2 eV, which corresponds to C=O in TMC300 (Xie et al. 2018). The aforementioned results indicate that the surfaces of

CNCs have been successfully combined with TMC300.

TGA was used to investigate the modifications effected by TMC300 on the thermal stability of pristine CNCs and mCNCs, and the TGA and DTA curves are depicted in Fig. 4. The onset degradation temperature, which is the temperature at 5% weight loss of pristine CNCs, was observed to be approximately 210.7 °C, and the weight loss can be attributed to absorbed water and sulfonate radical groups (Cha et al. 2012). On the other hand, TMC300 has a high onset temperature at approximately 296.6 °C, providing a basis to improve the thermal stability of CNCs. After modification by TMC300, the onset degradation temperatures of mCNCs with CNCs/TMC300 of 1:1 and 1:2 shift to 242.1 °C and 247.6 °C, respectively, exhibiting improvements by more than 30 °C compared to those of pristine CNCs.

According to the DTA curves, pristine CNCs exhibit a degradation process with three steps at the maximum weight loss temperatures (T_{max}) of 234.1 °C, 303.2 °C and 356.4 °C, respectively. The degradation processes of CNCs/TMC300 of 1/1 sample exhibit a degradation behavior similar to that of pristine CNCs, with a very small peak at 271.2 °C, and

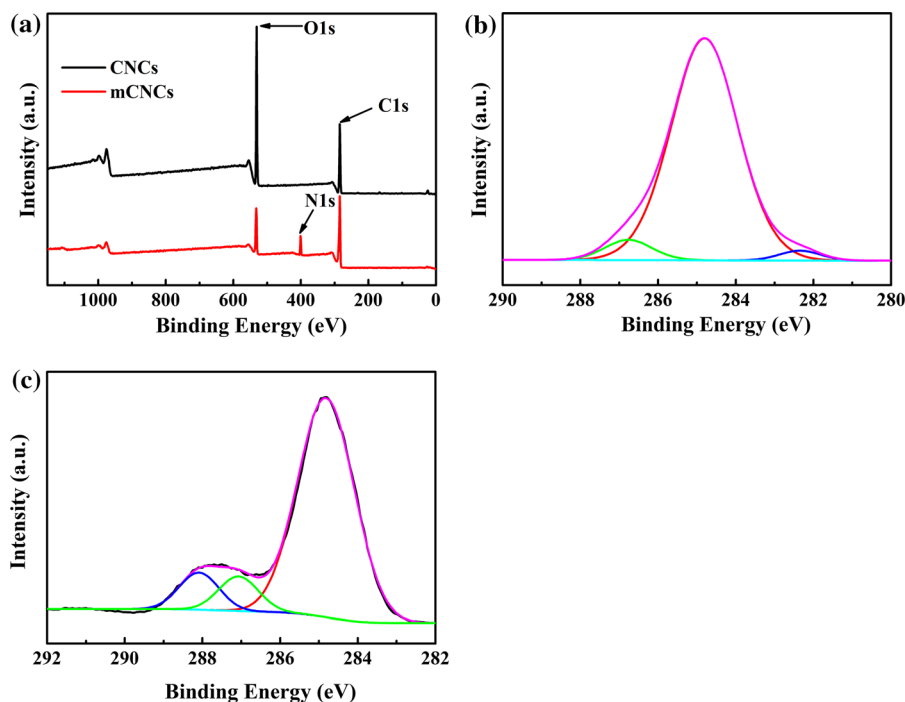


Fig. 3 XPS spectra of CNCs and mCNCs (a), and high-resolution XPS spectra of C1s for CNCs (b) and mCNCs (c)

Table 1 Binding energies (± 0.2 eV), corresponding assignment and, within brackets, atomic concentrations (%) for each peak fitted in XPS regions for CNCs and mCNCs. The error associated to the relative amounts does not exceed 5%

Samples	Atomic concentrations(%)				Content of the element(%)		
	C–O–C 282.4 eV	C–C, C–H 284.5 eV	C–O 287.0 eV	C=O 288.2 eV	C	O	N
CNCs	2.6	91.5	5.9	–	32.8	67.2	0
mCNCs	–	81.3	9.7	9.0	52.4	35.8	11.8

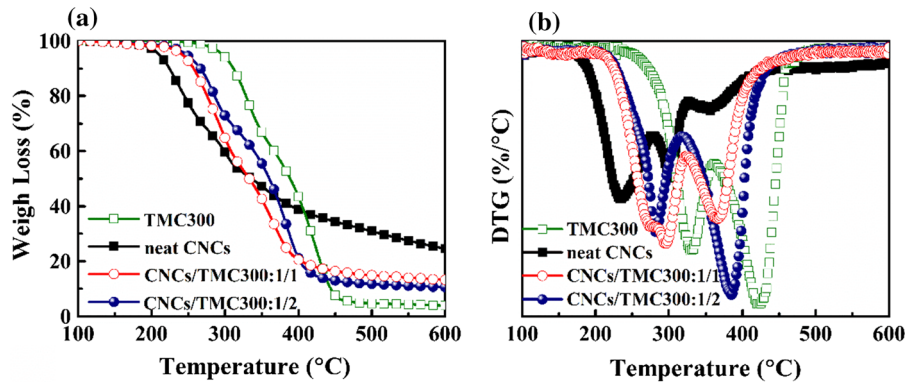


Fig. 4 a Thermogravimetric profiles of TMC300, CNCs, and mCNCs with the compositions of CNCs/TMC300: 1/1 and 1/2. b The corresponding derivative forms

two big peaks at 294.2 °C and 367.5 °C. However, the CNCs/TMC300 of 1/2 sample exhibit only two steps with T_{\max} at 277.5 °C and 383.2 °C, respectively. The diminishing of the first degradation peak implies that the degradation of absorbed water and sulfonate radical groups is weakened by the physisorption of TMC300. Therefore, the increased onset temperature and the changed degradation behaviors demonstrate that the physisorption of TMC300 significantly improves the thermal stability of CNCs. Considering the significant effects of CNCs/TMC300: 1/2 on the thermal stability, the mCNC samples with the compositions of CNCs/TMC300: 1/2 are used to prepare the PLLA/mCNC composites.

Crystallization behaviors of PLLA/CNC composites

As a type of self-assembly nucleation agent, TMC300 combined on the surface of cellulose is capable of greatly altering the crystallization behaviors of PLLA. Figure 5 depicts the crystallization morphologies of (a) PLLA, (b) PLLA/CNCs, (c) PLLA/TMC300, and (d) PLLA/1mCNCs during isothermal crystallization

at 140 °C for 30 min. The nucleation processes of these samples exhibited great differences among each other. No crystals for neat PLLA were observed in the first 100 s because of its long crystallization induction time (Auras et al. 2004). However, nuclei appeared during this time for all the modified PLLA samples, indicating that both CNCs and TMC300 can induce nucleation in PLLA. The numbers of crystal nuclei induced by each were different: the most were induced by PLLA/TMC300, followed by PLLA/1mCNCs and PLLA/CNCs. Another great difference is their crystallization morphologies. Neat PLLA and PLLA/CNC samples form spherulite structures with Maltese-crosses. However, the PLLA/TMC300 sample first forms large amounts of rod nuclei at 100 s, then appears as shish-kebab structures without evident Maltese-crosses (Fig. 5c₅), which is consistent with reports in existing literature (Bai et al. 2011). While the PLLA/1mCNC sample still forms spherulites with Maltese-crosses, the lamella exhibits shish-kebab structures (as depicted in the enlarged region in Fig. 5d₅). The aforementioned changes in crystallization behaviors suggest that the CNCs modified by

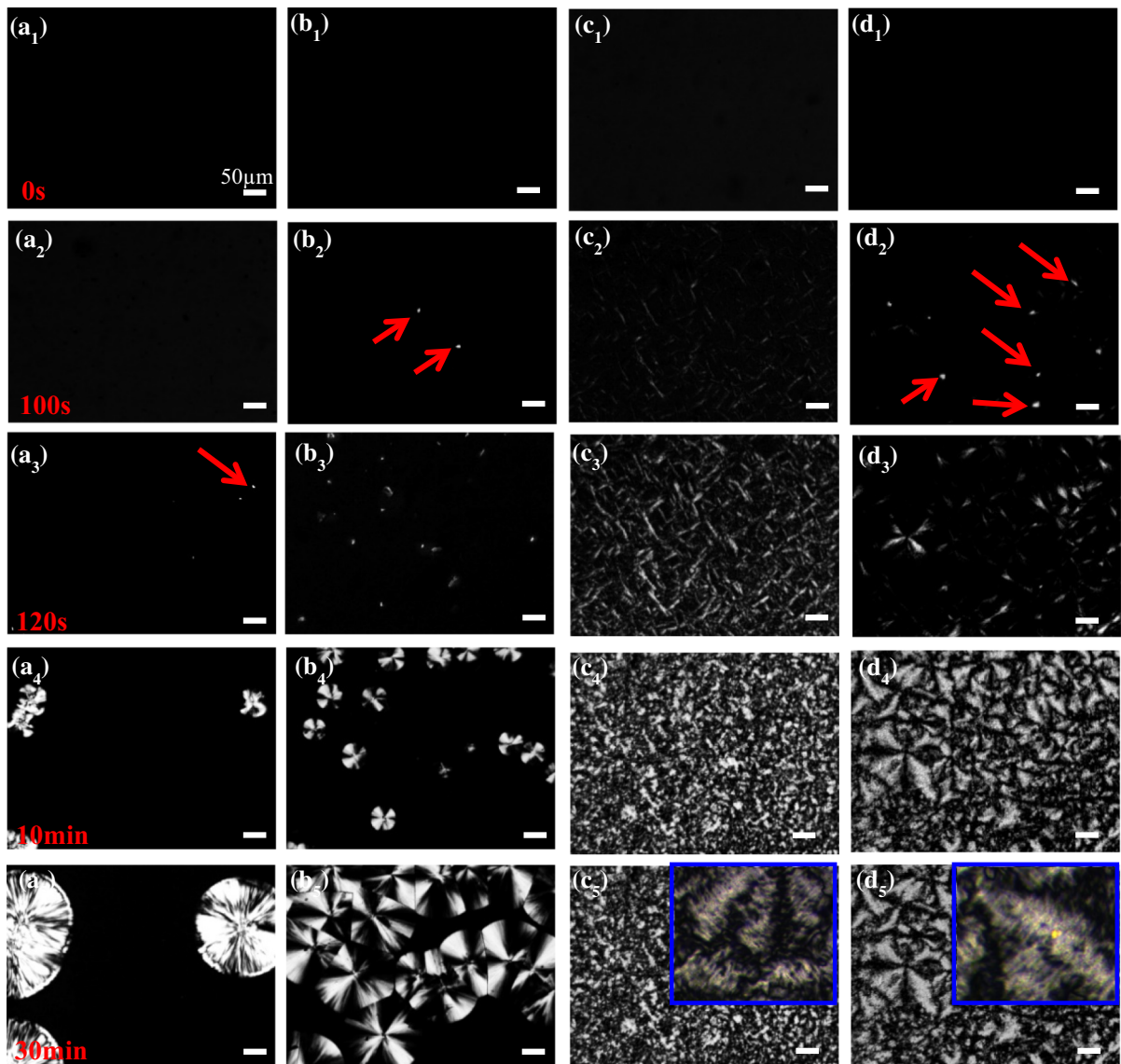


Fig. 5 In-situ POM images of **a** PLLA, **b** PLLA/CNCs, **c** PLLA/TMC300 and **d** PLLA/1mCNCs during isothermal crystallization at 140 °C for 30 min. The scale bar is 50 μm

TMC300 can improve the nucleation rate and change the crystallization morphology of PLLA.

Figure 6 depicts the DSC traces of PLLA, PLLA/CNCs, PLLA/1mCNCs and PLLA/TMC300 samples, (a) depicts cooling traces after erasing thermal history and (b) records the following heating traces. No crystallization exothermal peaks of PLLA and PLLA/CNCs are noticed during cooling process, while both PLLA/1mCNCs and PLLA/TMC300 samples exhibit exothermal peaks. This indicates that both mCNCs and TMC300 exert stronger nucleation effects than

pristine CNCs. However, the crystallization peak area of PLLA/1mCNCs is observed to be smaller than that of PLLA/TMC300, which reinforces the conclusion that CNCs and TMC300 have been successfully combined together.

All the samples exhibit pronounced glass transition temperatures (T_g) at approximately 64 °C during the heating process suggesting that the mobility of PLLA chains is not influenced by CNCs and TMC300. During this process, the incomplete crystallization during the cooling process continues to proceed and

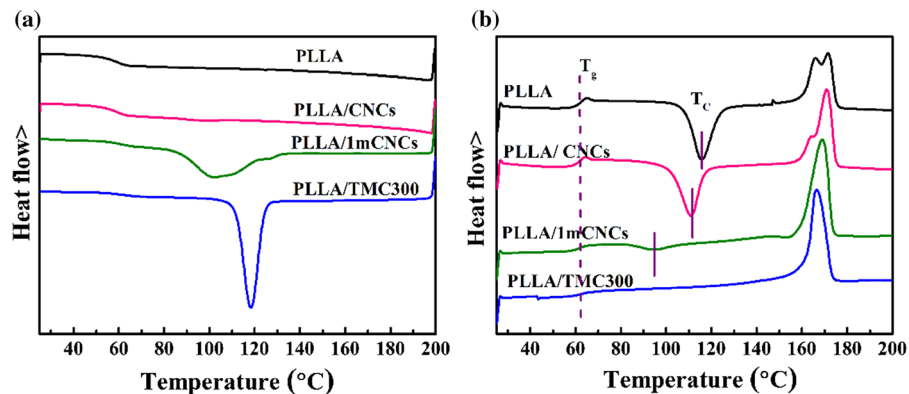


Fig. 6 DSC traces of PLLA, PLLA/CNCs, PLLA/TMC300, and PLLA/1mCNCs. **a** The cooling traces from 200 to 25 °C and **b** the heating 200 °C to 25 °C. The cooling and heating rates are both 10 °C/min

the exothermal peaks (T_c) for the PLLA, PLLA/CNCs, and PLLA/mCNCs samples appear at 116 °C, 111 °C, and 94 °C, respectively. The decreasing exothermal peak temperatures confirm that PLLA/mCNCs have a higher crystallization rate than PLLA/CNCs.

Mechanical properties of PLLA, PLLA/CNCs, and PLLA/mCNCs

The PLLA, PLLA/CNCs, and PLLA/mCNCs samples used to investigate mechanical properties were prepared via melt blending and their digital photos are presented in Fig. 7. After addition of pristine CNCs, the samples clearly become yellow-grey because of the decomposition of CNCs. However, few yellow dots are noticed in the PLLA/1mCNCs sample and small amounts yellow dots are noticed in the PLLA/3mCNC sample. This confirms that the thermal stability of CNCs was significantly improved by the physisorption of TMC300.

As mCNCs simultaneously improved the thermal stability of CNCs and changed the crystallization behaviors of PLLA, both of which positively impact the mechanical properties of PLLA/CNC composites, two kinds of samples were prepared to investigate the mechanical properties—sample without crystallization, which was prepared by quenching from melt to evaluate the effects of thermal stability, and sample with crystallization, which was obtained via slow cooling from melt to evaluate the effects of crystallization. Figure 8 depicts the WAXD spectrum of these samples. The spectrum separates into an amorphous peak and two crystalline peaks by virtue of

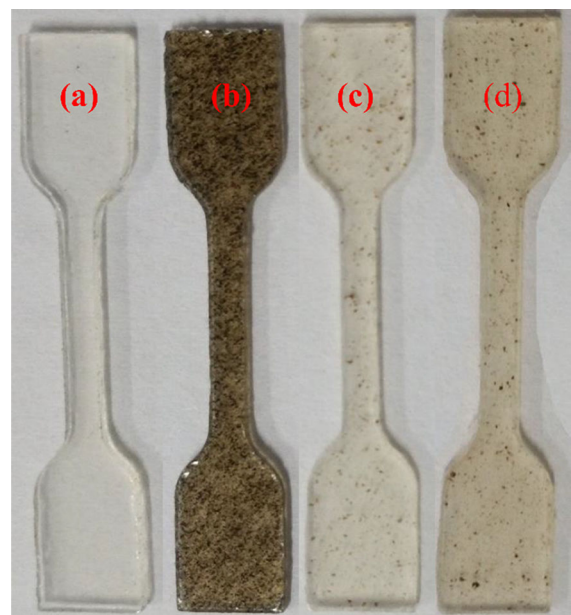


Fig. 7 Digital photographs of melt processing samples which are used for tensile experiments. **a** PLLA, **b** PLLA/CNCs, **c** PLLA/1mCNCs, and **d** PLLA/3mCNCs

Gaussian functions, and the crystallinities (x_c) were calculated based on the proportions of the areas of the crystalline peaks. No crystallization peaks were observed for the samples prepared by quenching. However, the samples prepared by slow cooling were observed to possess two characteristic diffraction peaks at 16.8° and 19°, which correspond to the α crystal of PLLA (Zhao et al. 2016). The crystallinity of PLLA was improved by the addition of CNCs and mCNCs. In accordance with the previous results of crystallization behaviors, PLLA/1mCNC samples

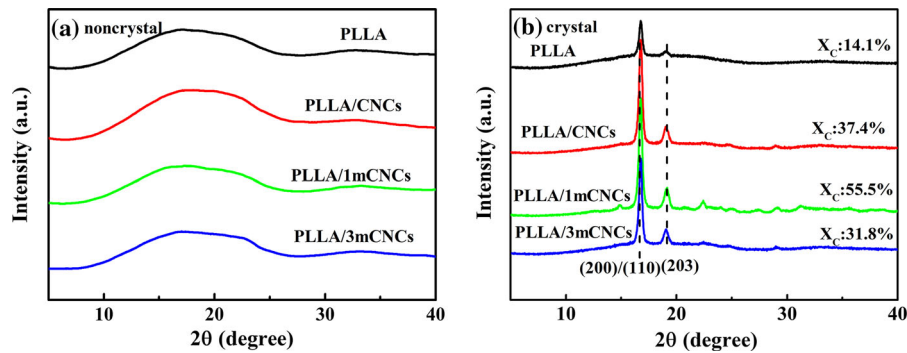


Fig. 8 WAXD spectra of PLLA, PLLA/CNCs, PLLA/1mCNCs, and PLLA/3mCNCs. The samples were prepared **a** by quenching from melt and **b** via naturally cooling from melt to the room temperature of 25 °C

exhibited higher crystallinity than PLLA/CNCs due to the nucleation effect of TMC300. The lower crystallinity of PLLA/3mCNCs can be attributed to the agglomeration of CNCs, which will be investigated via SEM.

The stress–strain diagram and data regarding the mechanical properties of the samples without crystallization are depicted in Fig. 9 and Table 2, respectively. The yielding strength, tensile strength, elongation at break, and tensile toughness of the PLLA/CNC sample are observed to be lower than those of the neat PLLA sample, with the only exception being the Young’s modulus. However, for the PLLA/1mCNC sample, all the mechanical parameters are observed to have increased, in particular, the elongation at break and tensile toughness, both of which increased by 33%. This reveals the significant enhancing and toughening effects of mCNCs on PLLA.

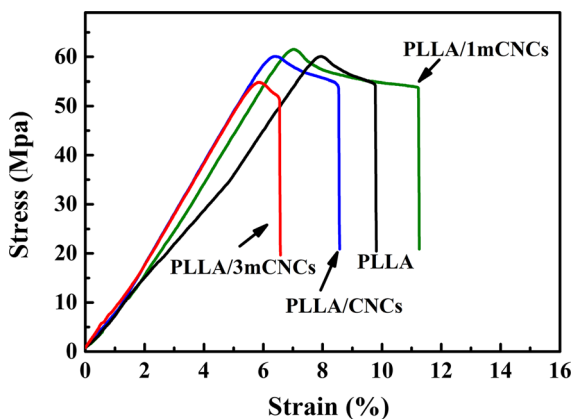


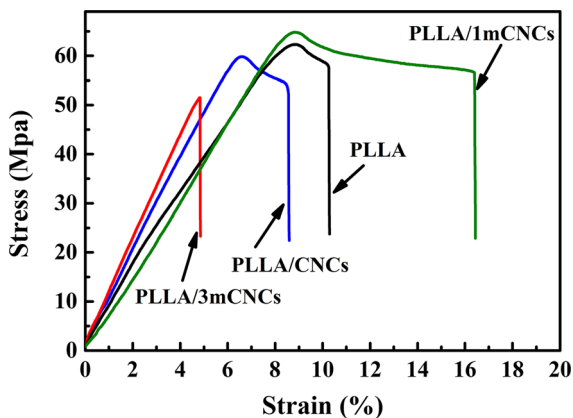
Fig. 9 Typical stress–strain diagram of PLLA, PLLA/CNCs, PLLA/1mCNCs, and PLLA/3mCNCs samples without crystallization

Compared to that of PLLA/CNCs, the lower Young’s modulus of PLLA/1mCNCs suggests that the nucleation agent TMC300 in mCNCs is incapable of increasing the modulus. However, the PLLA/3mCNC sample exhibited the highest Young’s modulus because it comprises a high proportion of CNCs. The decreased tensile performance of the PLLA/3mCNCs suggests that mCNCs might agglomerate at high contents. The changes in mechanical properties indicate that, as a kind of nanofiber, pristine CNCs cannot improve the tensile strength and elongation at break of PLLA by melt processing because of the decomposition of pristine CNCs. Nonetheless, after modification by physisorption of TMC300, it can simultaneously improve the tensile strength and toughness of PLLA.

Figure 10 and Table 3 depict the stress–strain diagram and the data regarding the mechanical properties of the samples with crystal structures. Compared to those of the samples without crystallization, the yielding strength, tensile strength, and Young’s modulus for the samples with the same composition are all observed to have slightly improved. As PLLA is in glass state at room temperature, this little improvement in mechanical properties is related with the small difference in mechanical properties between the glass state and crystalline state. However, for the PLLA/1mCNC sample, the elongation at break increases from 12.9% to 16.4%, which is an increase by 27%. In addition, the PLLA/3mCNC samples with a crystallinity of 31.8% (Fig. 8) only shows a very low elongation at break of 4.8% after crystallization. This contrary effect of mCNCs on the PLLA indicates that mCNCs bring about the significant changes in the structures of composites.

Table 2 The mechanical properties data of PLLA, PLLA/CNCs, PLLA/1mCNCs and PLLA/3mCNCs without crystallization

Samples	Yielding strength (MPa)	Tensile strength (MPa)	Elongation at break (%)	Young's modulus (MPa)	Tensile toughness(MJ/m ³)
PLLA	61.4 ± 0.9	53.7 ± 0.2	9.7 ± 1.6	687 ± 58	3.4 ± 0.7
PLLA/CNCs	56.9 ± 2.3	52.1 ± 1.4	7.8 ± 0.6	758 ± 23	3.2 ± 0.2
PLLA/1mCNCs	65.6 ± 1.9	56.7 ± 2.3	12.9 ± 2.2	696 ± 43	4.5 ± 0.2
PLLA/3mCNCs	54.7 ± 3.8	51.2 ± 3.3	6.55 ± 2.3	789 ± 82	2.0 ± 0.4

**Fig. 10** Typical stress–strain curves of PLLA, PLLA/CNCs, PLLA/1mCNCs, and PLLA/3mCNCs with crystal structures

Notched impact experiments were carried out to investigate the effects of CNCs or mCNCs and the results are recorded in Fig. 11. Unlike the tensile properties, the pristine CNCs also exhibit distinct toughening effect on PLLA for both crystallized and non-crystallized samples. However, after adding 1 wt% mCNCs, the toughness of crystallized sample and non-crystallized sample were improved by 65.7%

and 50%, respectively, compared to those of their neat PLLA samples. This difference reinforces the conclusion that the self-assembly character of TMC300 in mCNCs alters the micro-structures of the composites. For the PLLA/3mCNC samples, both kinds of samples exhibit a low impact strength at approximately 3.8 MPa, which is in accordance with the observed tensile properties.

In order to better analyze the effects of CNCs and mCNCs on the microstructures of PLLA, the SEM images of the composites have been presented in Fig. 12. Figure 12a depicts the morphologies of the samples without crystallization. The neat PLLA sample in Fig. 12a₁ exhibits a smooth and brittle fractured surface. For the PLLA/CNC sample depicted in Fig. 12a₂, some small white dots and holes were observed, which corresponded to the CNCs remaining in the matrix and pulled out of the matrix during fracture, respectively. Meanwhile, it is apparent that some aggregates of CNC particles (labeled with arrows) were unevenly dispersed in the matrix. On the other hand, for the PLLA/1mCNC sample (Fig. 12a₃), most CNCs were evenly dispersed in the matrix as indicated by the blue circles. Besides this, a

Table 3 The mechanical properties data of PLLA, PLLA/CNCs, PLLA/1mCNCs and PLLA/3mCNCs with crystal structure

Samples	Yielding strength (MPa)	Tensile strength (MPa)	Elongation at break (%)	Young's modulus (MPa)	Tensile toughness (MJ/m ³)
PLLA	62.9 ± 0.6	55.6 ± 1.3	9.8 ± 0.8	770 ± 20	3.9 ± 0.1
PLLA/CNCs	59.9 ± 2.5	53.9 ± 0.5	8.5 ± 1.3	850 ± 43	3.3 ± 0.8
PLLA/1mCNCs	64.5 ± 3.3	57.8 ± 1.4	16.4 ± 2.4	740 ± 33	7.5 ± 1.0
PLLA/3mCNCs	51.4 ± 4.3	51.5 ± 8.4	4.8 ± 1.6	865 ± 63	1.3 ± 0.3

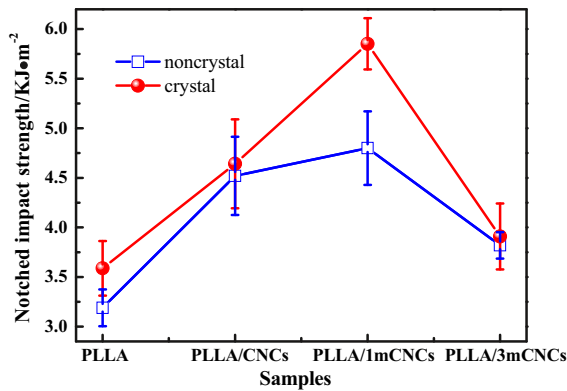


Fig. 11 The notched impact strength of PLLA, PLLA/CNCs, PLLA/1mCNCs, and PLLA/3mCNCs

small amount of aggregations of smaller sizes were also noticed, as labeled by arrows. However, for PLLA/3mCNC samples depicted in Fig. 12a₄, large numbers of white dots and holes with a larger sizes than that of PLLA/1mCNC sample (labeled with circles) were observed, which suggests poor dispersion of CNCs. In spite of this, the sizes of aggregations were observed to have significantly decreased compared to those of PLLA/CNCs. These changes demonstrate the capability of modified CNCs by TMC300 to improve the dispersion of CNCs in PLLA. However, when the content of mCNCs is high (reached 3 wt%), aggregations of CNCs still cannot be avoided. Therefore, the mechanical properties of PLLA/3mCNCs were not improved compared to those of PLLA.

Figure 12b depicts the microstructure images of the samples with crystal structure. To clearly observe the crystal structure, the crystallization samples were ultrasonically etched in an acetone/ethanol (1:1) mixed solution for 2 min before observation. Many spherulites are uncovered after etching for both the neat PLLA and PLLA/CNC samples, as depicted in Fig. 12b₁, b₂. After addition of mCNCs, a significant disappearance of spherulites is noticed (Fig. 12b₃, b₄). In the enlargement of Fig. 12b₃, one distinct line with an approximate length of 8 μm formed by self-assembly of TMC300 can be observed. Further, in the enlargement of Fig. 12b₄ of the PLLA/3mCNC sample, the shish-kebab morphologies across the lines can be clearly observed. The lines formed by TMC300 are similar to the morphologies that appeared in AFM image of modified CNCs. However, the sizes of these lines are much bigger than those depicted in the AFM image. Further, PLLA/1mCNCs exhibit spherulites with Maltese-crosses, as depicted in POM image (see in Fig. 5d₅), while the spherulites cannot be observed by SEM. The different morphologies suggest that the self-assembly process of nucleation agent is influenced by the groen space. The samples used to carry out AFM and POM experiments are thin films with a thickness of tens of nanometers or micrometers, and so the self-assembly process of TMC300 in mCNCs occurs in a confined space. Therefore, in the AFM results, the long lines parallel to CNCs are formed by TMC300 after complete self-assembly and the short lines perpendicular to CNCs are formed by incomplete self-assembly due to limited space. These incomplete

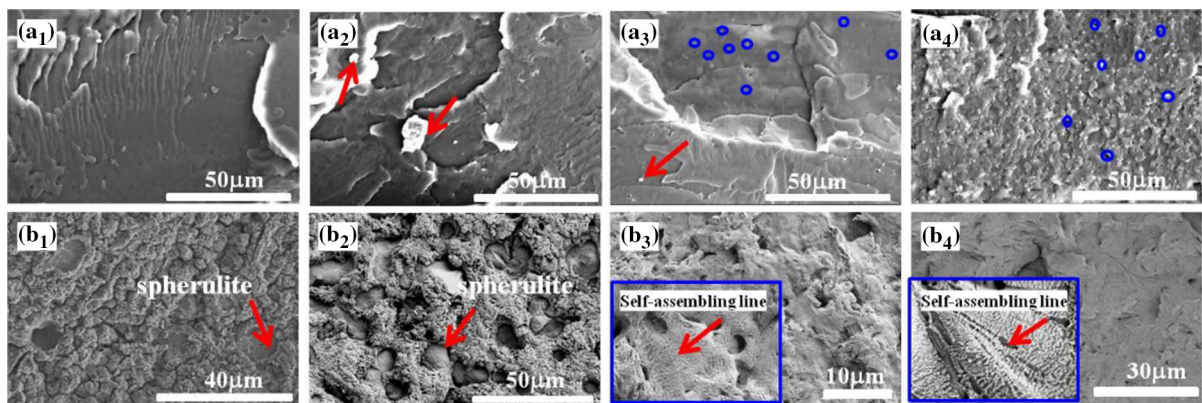


Fig. 12 SEM images of the composites with different compositions. Column (a) are samples without crystallization: **a**₁ PLLA, **a**₂ PLLA/CNCs, **a**₃ PLLA/1mCNCs and **a**₄ PLLA/

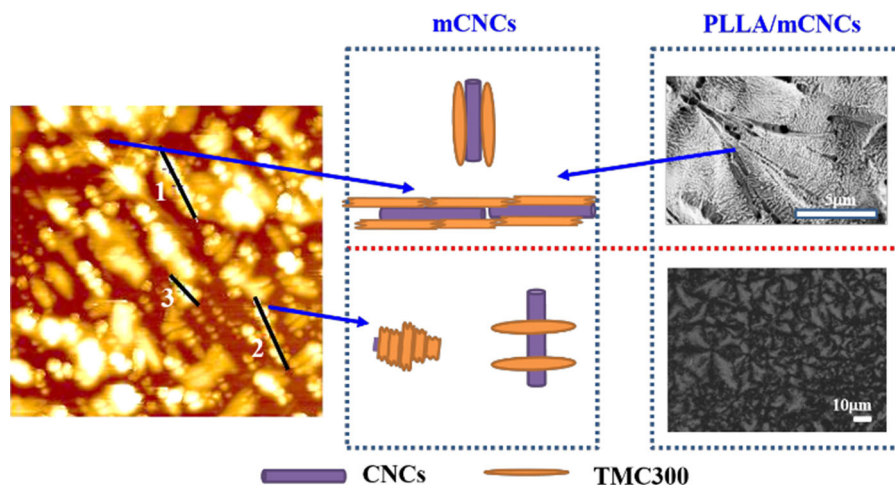
3mCNCs. Column (b) are samples with crystal structures: **b**₁ PLLA, **b**₂ PLLA/CNCs, **b**₃ PLLA/1mCNCs and **b**₄ PLLA/3mCNCs. The bottoms in (**b**₃) and (**b**₄) are the enlargements

self-assembly lines are incapable of changing the Maltese-cross spherulite morphology of PLLA in POM images. The samples used for SEM were prepared as thick films with the thickness of 0.6 mm, and the self-assembly could be completely completed in this environment, inducing the formation of long lines and the disappearance of spherulites. In both cases, the shish-kebab structures caused by TMC300 can be clearly observed.

The aforementioned results demonstrate that the self-assembly of mCNCs induce great effects on the microstructures and mechanical structures of PLLA/mCNC composites (as shown in Scheme 2). TMC300 is physically adsorbed on the surface of CNCs. Therefore, the sulfate is shielded and the thermal stability of CNCs is improved. During the crystallization process, self-assembly of TMC300 in mCNCs forms short lines or long lines depending on the growth space. When the growth space is confined in thin films, it mainly forms short lines perpendicular to CNCs and results in the formation of PLLA spherulites with shish-kebab lamella. When the growth space is unconfined in thick films, the combined TMC300 and CNCs in mCNCs form long lines under the effects of self-assembly of TMC300 and induce PLLA to form shish-kebab structures. These shish-kebab structures enhance the interface of PLLA/mCNC composites and transfer the stress efficiently, inducing the simultaneous improvement of tensile strength and toughness. Therefore, different to the reported work about PP/NF composites (Huang et al. 2017), in which self-assembly nucleation agent

formed “root” on the nature fibers, the mechanically interfacial lock in this work is the shish-kebab structure that was formed by nucleation agents and PLLA crystals at the interface of PLLA matrix and CNC filler.

Besides mechanical properties, improvement of heat resistance is another important task to increase the scope of the applications of PLLA. Dynamic mechanical analysis (DMA) was carried out to elucidate the effects of mCNCs on the heat resistance of the composites with crystal structures. Figure 13 depicts the changes in storage modulus, E' , with increasing temperature, for PLLA, PLLA/CNCs, and PLLA/1mCNCs. The E' values of all the samples dropped sharply in the temperature range of 60–80 °C due to glass transition. For PLLA and PLLA/CNC samples, subsequent increases in the value of E' at higher temperatures are related to cold crystallization caused by the DMA heating process. The E' corresponding to PLLA/1mCNCs does not exhibit such a change, suggesting that its crystallinity, formed in the primary thermal history, is high enough. More importantly, the E' of PLLA/1mCNCs at the whole temperature ranges is higher than that of PLLA and PLLA/CNCs. For example, at a temperature of 80 °C, E' of PLLA/1mCNCs is 348 MPa, while that of PLLA and PLLA/CNCs is 23 MPa and 75 MPa, respectively. The high E' values of PLLA/1mCNCs can be attributed to its high crystallinity effected by the modified CNCs, which can resist heat deflection at temperatures below the melting point of PLLA.



Scheme 2 Evolutions of mCNC microstructures in different growth spaces

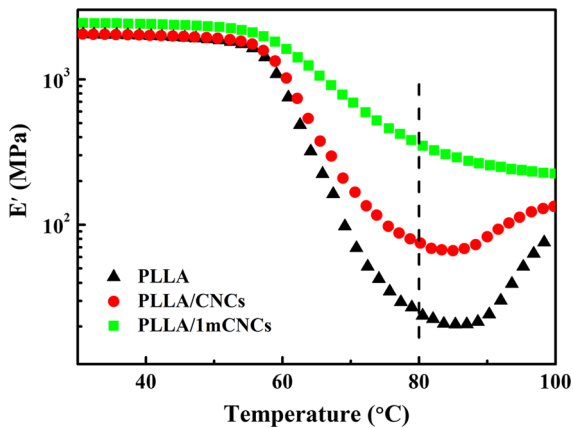


Fig. 13 Changes of storage modulus, E' as functions of temperature for PLLA, PLLA/CNCs, and PLLA/1mCNCs samples prepared by slow cooling. The heating rate is 2 °C/min

Conclusion

In summary, we prepared modified CNCs by adsorbing the self-assembly nucleation agent, TMC300, on its surface. Because the sulfonate of CNCs was shielded by TMC300, its thermal stability was significantly improved. This kind of modified CNCs can exhibit different self-assembly morphologies in confined and unconfined spaces, which influence the crystallization behaviors and microstructures of PLLA. Therefore, the crystallization rate of PLLA, the crystallinity and the heat resistance of PLLA/mCNC samples were all improved. And more importantly, modified CNCs induced shish-kebab structures in PLLA/mCNC samples, which enhanced the interface as a mechanically interfacial lock and improved the mechanical properties. Therefore, these results indicate that we can take full advantage of CNCs via this physical method to modify PLLA or other semi-crystalline polymers.

Acknowledgments This work was supported by the National Natural Science Foundation, China (Grant No. 51503117).

References

- Abitbol T, Kloser E (2013) Estimation of the surface sulfur content of cellulose nanocrystals prepared by sulfuric acid hydrolysis. *Cellulose* 20:785–794
- Al-Itry R, Lamnawar K, Maazouz A (2012) Improvement of thermal stability, rheological and mechanical properties of PLA, PBAT and their blends by reactive extrusion with functionalized epoxy. *Polym Degrad Stab* 97:1898–1914
- Auras R, Harte B, Selke S (2004) An overview of polylactides as packaging materials. *Macromol Biosci* 4:835–864
- Azouz KB, Ramires EC, den Fonteyne WV, Kissi NE, Dufresne A (2013) Simple method for the melt extrusion of a cellulose nanocrystal reinforced hydrophobic polymer. *ACS Macro Lett* 1:236–240
- Bai H, Zhang W, Deng H, Zhang Q, Fu Q (2011) Control of crystal morphology in poly(L-lactide) by adding nucleating agent. *Macromolecule* 44:1233–1237
- Bao R, Chrisey DB (2010) Chemical states of carbon in amorphous boron carbide thin films deposited by radio frequency magnetron sputtering. *Thin Solid Films* 51:164–168
- Bashar MM, Zhu H, Yamamoto S, Mitsuishi M (2019) Highly carboxylated and crystalline cellulose nanocrystals from jute fiber by facile ammonium persulfate oxidation. *Cellulose* 26:3671–3684
- Bhardwaj R, Mohanty AK (2007) Modification of brittle polylactide by novel hyperbranched polymer-based nanostructures. *Biomacromolecules* 8:2476–2484
- Börjesson M, Sahlin K, Bernin D, Westman G (2017) Increased thermal stability of nanocellulose composites by functionalization of the sulfate groups on cellulose nanocrystals with azetidinium ions. *J Appl Polym Sci* 135:45963
- Boujemaoui A, Sanchez CC, Engström J, Bruce C, Fogelström L, Carlmark A, Malmström E (2017) Polycaprolactone nanocomposites reinforced with cellulose nanocrystals surface-modified via covalent grafting or physisorption: a comparative study. *ACS Appl Mater Interfaces* 9:35305–35318
- Brinatti C, Huang J, Berry RM, Tam KC, Loh W (2016) Structural and energetic studies on the interaction of cationic surfactants and cellulose nanocrystals. *Langmuir* 32:689–698
- Cha R, He Z, Ni Y (2012) Preparation and characterization of thermal/pH-sensitive hydrogel from carboxylated nanocrystalline cellulose. *Carbohydr Polym* 88:713–718
- Cheng M, Qin Z, Chen Y, Hu S, Ren Z, Zhu M (2017) Efficient extraction of cellulose nanocrystals through hydrochloric acid hydrolysis catalyzed by inorganic chlorides under hydrothermal conditions. *ACS Sustain Chem Eng* 5:4656–4664
- Choi JE, Park J, Park DW, Shim SE (2010) MWCNT–OH adsorbed electrospun nylon 6,6 nanofibers chemiresistor and their application in low molecular weight alcohol vapours sensing. *Synth Met* 160:2664–2669
- Dash TK, Konkimalla VB (2012) Poly- ϵ -caprolactone based formulations for drug delivery and tissue engineering: a review. *J Control Release* 158:15–33
- Dhar P, Bhardwaj U, Kumar A, Katiyar V (2015) Poly (3-hydroxybutyrate)/cellulose nanocrystal films for food packaging applications: barrier and migration studies. *Polym Eng Sci* 55:2388–2395
- Fang H, Chen X, Wang S, Cheng S, Ding Y (2019) Enhanced mechanical and oxygen barrier performance in biodegradable polyurethanes by incorporating cellulose nanocrystals with interfacial polylactide stereocomplexation. *Cellulose* 26:9751–9764

- Fortunati E, Peltzer M, Armentano I, Torre L, Jiménez A, Kenny JM (2012) Effects of modified cellulose nanocrystals on the barrier and migration properties of PLA nano-bio-composites. *Carbohydr Polym* 90:948–956
- Gan L, Wang Y, Zhang M, Xia X, Huang J (2019) Hierarchically spacing DNA probes on bio-based nanocrystal for spatial detection requirements. *Sci Bull* 64:934–940
- Góis GS, Nepomuceno NC, França CHA, Almeida YMB, Hernández EP, Oliveira JF, Oliveira MP, Santo ASF (2019) Influence of morphology and dispersion stability of CNC modified with ethylene oxide derivatives on mechanical properties of PLLA-based nanocomposites. *Polym Compos* 40:399–408
- Gupta A, Simmons W, Schueneman GT, Mintz EA (2016) Lignin-coated cellulose nanocrystals as promising nucleating agent for poly(lactic acid). *J Therm Anal Calorim* 126:1243–1251
- Gupta A, Simmons W, Schueneman GT, Hylton D, Mintz EA (2017) Rheological and thermo-mechanical properties of poly(lactic acid)/lignin-coated cellulose nanocrystal composites. *ACS Sustain Chem Eng* 5:1711–1720
- Habibi Y (2014) Key advances in the chemical modification of nanocelluloses. *Chem Soc Rev* 43:1519–1542
- Han J, Zhou C, Wu Y, Liu F, Wu Q (2013) Self-assembling behavior of cellulose nanoparticles during freeze-drying: effect of suspension concentration, particle size, crystal structure, and surface charge. *Biomacromolecules* 14:1529–1540
- He X, Li Y, Nie M, Wang Q (2016) Root-like glass fiber with branched fiber prepared via molecular self-assembly. *RSC Adv* 6:45492–45494
- Helbert W, Cavaille JY, Dufresne A, Fourier UJ (1996) Thermoplastic nanocomposites filled with wheat straw cellulose whisker. Part 1: processing and mechanical behavior. *Polym Compos* 17:604–611
- Huang P, Shi S, Liu Y, Nie M, Wang Q (2017) Root-like natural fibers in polypropylene prepared via directed diffusion and self-assembly driven by hydrogen bonding. *RSC Adv* 7:32193–32197
- Incarinato L, Acierno D, Russo P, Malinconico M, Laurienzo P (1999) Influence of composition on properties of nylon 6/EVOH blends. *J Polym Sci Part B Polym Phys* 37:2445–2455
- Jin X, Heepe L, Strueben J, Adelung R, Gorb SN, Staubitz A (2014) A Challenges and solutions for joining polymer materials. *Macromol Rapid Commun* 35:1551–1570
- Kong W, Zhu B, Su F, Wang Z, Shao C, Wang Y, Liu C, Shen C (2019) Melting temperature, concentration and cooling rate-dependent nucleating ability of a self-assembly aryl amide nucleator on poly(lactic acid) crystallization. *Polymer* 168:77–85
- Li H, Huneault MA (2007) Effect of nucleation and plasticization on the crystallization of poly(lactic acid). *Polymer* 48:6855–6866
- Liu C, Jin R, Ouyang X, Wang Y (2017) Adsorption behavior of carboxylated cellulose nanocrystal-polyethyleneimine composite for removal of Cr(VI) ions. *Appl Surf Sci* 408:77–87
- Lu J, Tappel RC, Nomura CT (2009) Mini-review: biosynthesis of poly(hydroxyalkanoates). *Polym Rev* 49:226–248
- Mano V, Chimenti S, Ruggri G, Pereira FV, Oaula EL (2017) P(CL-b-LLA) diblock copolymers grafting onto cellulosic nanocrystals. *Polym Bull* 74:3673–3688
- Mariano M, Pilate F, Oliveira FB, Khelifa F (2017) Preparation of cellulose nanocrystal-reinforced poly(lactic acid) nanocomposites through noncovalent modification with PLLA-based surfactants. *ACS Omega* 2:2678–2688
- Montes S, Etxeberria A, Mocholi V, Rekondo A, Grande H, Labidi J (2018) Effect of combining cellulose nanocrystals and graphene nanoplatelets on the properties of poly(lactic acid) based films. *Exp Polym Lett* 12:543–555
- Morin A, Dufresne A (2002) Nanocomposites of chitin whiskers from *rifit* tubes and poly(caprolactone). *Macromolecules* 35:2190–2199
- Nan F, Nagarajan S, Chen Y, Liu P, Duan Y, Meng Y, Zhang J (2017) Enhanced toughness and thermal stability of cellulose nanocrystal iridescent films by alkali treatment. *ACS Sustain Chem Eng* 5:8951–8958
- Nie M, Kalyon DM, Fisher FT (2014) Interfacial load transfer in polymer/carbon nanotube nanocomposites with a nanohybrid shish kebab modification. *ACS Appl Mater Interf* 6:14886–14893
- Pal N, Dubey P, Gopinath P, Pal K (2017) Combined effect of cellulose nanocrystal and reduced graphene oxide into polylactic acid matrix nanocomposite as a scaffold and its anti-bacterial activity. *Int J Biol Macromol* 95:94–105
- Petersson L, Kvien I, Oksman K (2007) Structure and thermal properties of poly(lactic acid)/cellulose whiskers nanocomposite materials. *Compos Sci Technol* 67:2535–2544
- Ramot Y, Haim-Zada M, Domb AJ, Nyska A (2016) Biocompatibility and safety of PLA and its copolymers. *Adv Drug Deliv Rev* 107:153–162
- Raquez JM, Murena Y, Goffin AL, Habibi Y, Ruelle B, DeBuyl F, Dubois P (2012) Surface-modification of cellulose nanowhiskers and their use as nanoreinforcers into polylactide: a sustainably-integrated approach. *Compos Sci Technol* 72:544–549
- Roman M, Winter WT (2004) Effect of sulfate groups from sulfuric acid hydrolysis on the thermal degradation behavior of bacterial cellulose. *Biomacromolecules* 5:1671–1677
- Samir MASA, Allein F, Gorecki W, Sanchez JY, Dufresne A (2004) Nanocomposite polymer electrolytes based on poly(oxyethylene) and cellulose nanocrystals. *J Phys Chem B* 108:10845–10852
- Shi J, Liu W, Jiang X, Liu W (2019) Preparation of cellulose nanocrystal from tobacco-stem and its application in ethyl cellulose film as a reinforcing agent. *Cellulose*. <https://doi.org/10.1007/s10570-019-02904-0> (online)
- Shojaeiarani J, Bajwa DS, Stark NM (2018) Green esterification: a new approach to improve thermal and mechanical properties of poly(lactic acid) composites reinforced by cellulose nanocrystals. *J Appl Polym Sci* 135:46468
- Snell KD, Peoples OP (2009) PHA bioplastic: a value-added coproduct for biomass biorefineries. *Biofuels Bioprod Bioref* 3:456–467
- Šturcova A, Davies GR, Eichhorn SJ (2005) Elastic modulus and stress-transfer properties of tunicate cellulose whiskers. *Biomacromolecules* 6:1055–1061

- Tan X, Hamid SBA, Lai CW (2015) Preparation of high crystallinity cellulose nanocrystals (CNCs) by ionic liquid solvolysis. *Biomass Bioenergy* 81:584–591
- Voronova MI, Surov OV, Zakharov AG (2013) Nanocrystalline cellulose with various contents of sulfate groups. *Carbohydr Polym* 98:465–469
- Wang N, Ding E, Cheng R (2007) Thermal degradation behaviors of spherical cellulose nanocrystals with sulfate groups. *Polymer* 48:3486–3493
- Wen L, Xin Z, Hu D (2010) A new route of manipulation of poly(L-lactic acid) crystallization by self-assembly of p-tert-butylcalix[8]arene and toluene. *J Polym Sci Part B Polym Phys* 48:1235–1243
- Xie Q, Wang S, Chen X, Zhou Y, Fang H, Li X, Cheng S, Ding Y (2018) Thermal stability and crystallization behavior of cellulose nanocrystals and their poly(L-lactide) nanocomposites: effects of surface ionic group and poly(D-lactide) grafting. *Cellulose* 25:6847–6862
- Yang J, Wang X, Liang R, Kong R, Sun Y, Tang J, Li L, Xue L, Chen Q (2018) Polymorphism, thermal stability and enzymatic degradation of poly(1,4-butylene adipate) tailored by a benzene-1,3,5-tricarboxamide-based nucleating agent. *J Mater Sci* 53:10569–10581
- Zhang C, Salick MR, Cordie TM, Ellingham T, Dan Y, Turng LS (2015) Incorporation of poly(ethylene glycol) grafted cellulose nanocrystals in poly(lactic acid) electrospun nanocomposite fibers as potential scaffolds for bone tissue engineering. *Mater Sci Eng C* 49:463–471
- Zhao L, Li Q, Zhang R, Tian X, Liu L (2016) Effects of functionalized graphenes on the isothermal crystallization of poly(L-lactide) nanocomposites. *Chin J Polym Sci* 34:111–121

Publisher's Note Springer Nature remains neutral with regard to jurisdictional claims in published maps and institutional affiliations.